FACTA UNIVERSITATIS
Series:**Mechanical Engineering** Vol. 20, Nº 2, 2022, pp. 211 - 235
https://doi.org/10.22190/FUME220221011H

Original scientific paper

THE CARBON NANOTUBE-EMBEDDED BOUNDARY LAYER THEORY FOR ENERGY HARVESTING

Ji-Huan He[1,2,3], Nader Y. Abd Elazem[4]

[1]School of Civil Engineering, Xi'an University of Architecture & Technology, Xi'an, China
[2]National Engineering Laboratory for Modern Silk, College of Textile and Clothing Engineering, Soochow University, Suzhou, China
[3]School of Science, Xi'an University of Architecture and Technology, Xi'an, China
[4]Department of Basic Science, Pyramids HigherInstitute for Engineering and Technology, 6thof October City, Giza, Egypt

Abstract. *Single-walled carbon nanotubes (SWNTs)and multi-walled nanotubes (MWNTs) are gaining appeal in mechanical engineering and industrial applications due to their direct influence on enhancing the thermal conductivity of base fluids. With such intriguing properties of carbon nanotubes in mind, our goal in this work is to investigate radiation effects on the flow of carbon nanotube suspended nanofluids in the presence of a magnetic field past a stretched sheet impacted by slip state. CNTs flow and heat transmission are frequently modelled in practice using nonlinear differential equation systems. This system has been precisely solved, and an accurate analytical expression for the fluid velocity in terms of an exponential function has been derived, while the temperature distribution is stated in terms of a confluent hypergeometric function. The impact of the radiation parameter, slip parameter, sloid volume fraction, magnetic parameter, Eckart and Prandtl numbers on the velocity, temperature, and heat transfer rate profiles are demonstrated using a parametric analysis. When compared to the two types of nanoparticles (Cooper and Silver) in earlier published articles, temperature profiles for single-walled nanotubes (SWNTs) and multi-walled nanotubes (MWNTs) are revealed to be particularly sensitive to radiation, solid volume fraction, and slip parameters. Nanomechanical gears, nanosensors, nanocomposite materials, resonators, and thermal materials are only a few of the present problem's technical applications.*

Key words: *Nanofluids, Single-walled nanotubes, Multi-walled nanotubes, Radiation, Slip condition, Stretching sheet*

Received: February 20, 2022 / Accepted March12, 2022
Corresponding author: Nader Y. Abd Elazem
Department of Basic Science, Pyramids Higher Institute for Engineering and Technology,6th of October City, Giza 12578, Egypt
E-mail: naderelnafrawy@yahoo.com, nader_47@hotmail.com

1. INTRODUCTION

CNTs have obtained a lot of interest in the last decades because of their amazing mechanical and electrical capabilities [1-3]. Indeed, they are known to have very high thermal conductivity [4-5], therefore liquids containing CNTs are predicted to boost heat transfer near the laminar boundary layer. Carbon nanotubes are cylinder-shaped nanostructures, which have exceptional properties that make them helpful in mechanical engineering, optics, electronics, nanotechnology, and materials science [6].

Zuo and Liu [7] offered various unique concepts for graphene/SiC composites for the first time, including the graphene fractal and two-scale porosity. Theoretical investigations show that graphene concentration and two-scale fractal dimensions have a considerable influence on the mechanical and electrical properties of graphene/SiC composites.

CNTs are either a graphite sheet coiled into a nanoscale tube (single-wall carbon nanotubes (SWCNTs)) or multiple graphene tubes wrapped around the core of the SWCNT (multi-wall carbon nanotubes (MWCNTs)).

CNTs feature unique physical and chemical qualities [8] such as thermal and magnetic performance, as well as unique optical properties. Ref. [9] studied the effect of carbon nanotubes on total heat transfer performance in nucleate boiling, which occurs in power plant boilers and evaporators, as well as refrigeration and air-conditioning equipment, and it was discovered that CNTs' infiltration into the thermal boundary layer can form more bubbles at the surface, and this can enhance nucleate boiling heat transfer. Carbon nanotubes (CNTs) are one of the most promising nanomaterials [10]. Single-walled carbon nanotubes (SWCNTs) and multi-walled carbon nanotubes (MWCNTs) are the most often utilized CNTs [11].

Xue [12] presented a novel model of CNTs effective thermal conductivity to reveal theoretically CNTs excellent heat transfer performance. These findings are in good accord with the experimental data. Carbon nanotubes (CNTs) have received a lot of interest in recent years because of their remarkable electrical and mechanical capabilities [7, 13]. In Ref. [14], an analysis was presented to study the actual and theoretical properties of CNTs thermal conductivity. According to Ref. [15], SWCNTs have a higher thermal conductivity of up to 15% than other nanoparticle-based nanofluids. The authors of [16] explored the influence of SWCNTs on the presence of saltwater and water with solar radiation energy under varied stream conditions. CNTs have roughly six times the heat conductivity of common materials at normal temperature, according to the findings of a study published in [17]. Using two different types of carbon nanotubes (SWCNTs and MWCNTs), Ref. [18] studied the peristaltic flow of carbon nanotubes in an asymmetric channel with temperature and velocity slip effects. In terms of magnetic field and solid volume percentage, it is discovered that the velocity field for SWCNT is bigger than that of MWCNT.

The results of the experimental study in Ref. [19] showed the relevance of rheological characterization in establishing the presence and structural information of nanofluid forms, which can assist in the understanding of the thermal properties of such materials. Analysis was provided in Ref. [20] to discuss the peristaltic flow and heat transfer of carbon nanotubes in a diverging tube. It is found that the velocity field for SWCNT is greater as compared to the MWCNT and the size and no of trapped bolus decreases for MWCNT when we compared with the SWCNT.

Khan et al. [21] present a complete analysis of the influence of hybrid nano-fluid (ferrous oxide water and carbon nanotubes) CNTs-Fe_3O_4, H_2O between two parallel plates with a varying magnetic field. It has been noticed that the increase in the volume fraction of the nano-

material significantly fluctuates the velocity profile near the channel wall due to an increase in the fluid density. In addition, single-wall nanotubes have a greater effect on temperature than multi-wall carbon nanotubes. Statistical analysis shows that the fraction of the nano-material significantly fluctuates the velocity profile near the channel wall due to an increase in the fluid density. Statistical analysis shows that the thermal flow rate of (Fe_3O_4-SWCNTs-water) and (Fe_3O_4-MWCNTs-water) rises from 1.6336 per cent to 6.9519 per cent, and 1.7614 per cent to 7.4413 per cent, respectively when the volume fraction of nanomaterial increases from 0.01 to 0.04. Many authors have studied the flow and heat transmission of ordinary nanoparticles and suspended carbon-nanotube nanofluids. For instance, the authors of Ref. [22] studied the heat transfer behaviour of CNT nanofluids flowing through a horizontal tube. They discovered that the increase of convective heat transfer is dependent on the Reynolds number and solid volume fraction of CNTs.

He and Abd Elazem [23] investigated the impact of partial slips and temperature jumps on heat and mass transport in a boundary layer nanofluid flowing over a stretched or shrinking surface.

It is found that the slip parameter improves the temperature field and increases the thermal boundary layer thickness, as well as the concentration function's boundary layer thickness in the case of a stretched sheet. When the slip parameter is raised in the case of the shrinking sheet, the dual solutions for temperature and concentration functions are reduced. Thermal conductivity becomes more important at high working temperatures in common applications such as materials engineering and electronic parts. Thermal efficiency is described in physics as a material's purpose of transporting heat. This can be seen clearly from Fourier's heat transfer theorem. Theoretical and practical problems, such as a continuous supply of thermal energy, are growing rapidly. Radiation heat transfer research is crucial in high-temperature industrial applications.

Abd Elazem and Elgazery [24] examined the impacts of variable viscosity and thermal radiation for a mixed convective heat and mass transfer nanofluid flow along a vertical wavy surface. It is revealed that when the temperature of the radiation increases, the nanoparticle concentration curves near the wavy surface decrease while the far-field increases. Further, when the radiation parameter rises, so should the thermal boundary layer. Importantly, the variable viscosity parameter boosts the steady-state axial nanofluid velocity profile at the wavy surface boundaries while decreasing it further away. Many additional relevant results are also mentioned in the references [25-28].

As a result, the current work intends to explore the influence of the radiation parameter and the boundary condition of partial slip on the flow of carbon nanotubes suspended nanofluids across a stretched sheet in the presence of a magnetic field. The physical model is solved using an appropriate analytical solution for fluid velocity in terms of an exponential function and a confluent hypergeometric function for temperature distribution, which are searched and compared to previously published findings, notably [29]. The effect of the included physical parameters on the flow and heat transfer characteristics of carbon nanotube suspended nanofluids, as well as Cu-water and Ag-water nanofluids, is depicted graphically. The results of this study indicate that the thickness of the thermal barrier layer of the heat transfer rate rises as the radiation parameter increases, for the stretching sheet, thereby reducing the heat transfer rate.

The findings have a wide range of applications, including thermal- mechanical effects in high-speed flights, rockets, nuclear reactors and design of a solar energy collector's heat transfer in Refs. [23, 30-31].

2. MATHEMATICAL MODEL OFFLOW AND HEAT TRANSFER

The PDEs that characterize the flow and similarity transformations are described in detail in Ref. [29]; they are not included here to avoid duplication. The flow and heat transfer of an incompressible viscous nanofluid containing single- and multi-wall carbon nanotubes across a linearly semi-infinite stretched sheet will be investigated using the radiation term in the article [32] and the slip condition specified in Eq. (3) below to modify in [29]. As a result, the final state is governed by the following system of nonlinear differential equations under the influence of the radiation parameter, slip parameter, and a constant magnetic field:

$$f'''(\eta) - \overline{C_1}[f'^2(\eta) - f(\eta) f''(\eta) + \frac{M}{\overline{C_2}} f'(\eta)] = 0, \tag{1}$$

$$(1+R)g''(\eta) - \Pr \frac{k_f}{k_{nf}} \overline{C_3}[2 f'(\eta) g(\eta) - f(\eta) g'(\eta) - \frac{Ec}{\overline{C_4}} (f''(\eta))^2] = 0. \tag{2}$$

The slip modifies the boundary conditions in Ref. [29] as follows:

$$f(0) = 0,\ f'(0) = d + Lf''(0),\ f'(\infty) = 0, g(0) = 1, g(\infty) = 0, \tag{3}$$

where the prime implies differentiation with respect to η, $f(\eta)$ and $g(\eta)$ are the dimensionless of the stream and temperature functions, respectively, η is the similarity variable, and L is the velocity slip parameter. Furthermore, Pr, M and Ec are the Prandtl number, magnetic parameter, and Eckert number, as stated in Ref. [29]. Also, as indicated in Ref. [32], R is the radiation parameter, d = 1 signifies a stretched sheet, and $\overline{C_i}, (i = 1,...,4)$ are defined as

$$\begin{aligned} &\overline{C_1} = (1-\phi)^{2.5}(1-\phi+\phi\frac{\rho_{CNT}}{\rho_f}), \overline{C_2} = (1-\phi+\phi\frac{\rho_{CNT}}{\rho_f}), \\ &\overline{C_3} = (1-\phi+\phi\frac{(\rho C_p)_{CNT}}{(\rho C_p)_f}),\ \overline{C_4} = (1-\phi)^{2.5}(1-\phi+\phi\frac{(\rho C_p)_{CNT}}{(\rho C_p)_f}). \end{aligned} \tag{4}$$

The thermophysical characteristics of single- and multi-wall carbon nanotubes are shown in Table 1. Furthermore, the heat conductivity of single- and multi-wall CNTs is discussed in Xue's study as follows [12]:

$$\frac{k_{nf}}{k_f} = \frac{1-\phi+2\phi\left(\frac{k_{CNT}}{k_{CNT}-k_f}\right)\ln\left(\frac{k_{CNT}+k_f}{2k_f}\right)}{1-\phi+2\phi\left(\frac{k_f}{k_{CNT}-k_f}\right)\ln\left(\frac{k_{CNT}+k_f}{2k_f}\right)}. \tag{5}$$

It is known that ϕ is the solid volume fraction of the single- and multi-wall CNTs, ρ_f and ρ_{CNT} are the densities, $(\rho C_p)_f$ and $(\rho C_p)_{CNT}$ are the heat capacitances, k_f and k_{CNT} are the thermal conductivities, $(k)_f$ and $(k)_{CNTs}$ denote the basic fluid and solid fractions, and k_{nf} is the thermal conductivity, respectively.

Table 1 Water's and nanoparticles' thermophysical characteristics [12]

Physical properties	ρ (kg / m³)	C_p (J / kg K)	k (W /m k)
Fluid phase (Water)	997.1	4179	0.613
SWCNT	2600	796	6600
MWCNT	1600	235	3000

Engineering flow behavior is very significant in materials treatment processes for the local skin friction coefficient, C_f, and the Nusselt number, Nu_x. Here are the formulations for the local skin friction coefficient, C_f, and the Nusselt number, Nu_x.

$$C_f(1-\phi)^{2.5}\sqrt{\mathrm{Re}_x} = -2f''(0),\ \frac{Nu_x}{\mathrm{Re}_x}\left(\frac{k_f}{k_{nf}}\right) = -g'(0). \tag{6}$$

Where Re_x represents the local Reynolds number defined in Ref. [29]. Furthermore, when R=L=0, the system of Eqs. (1) to (3) yields to [29].

2.1. Exact Solutions

The precise solutions of the system of Eqs. (1) and (2) with boundary conditions Eq. (3) are found in this section. Assume the f-differential Eq. (1) has a solution that fulfils the boundary condition Eq. (3) in the following form:

$$f(\eta) = n + me^{-\bar{\beta}\eta}. \tag{7}$$

From Eq. (7), we may derive that the boundary requirements for $f(\eta)$ are provided in Eq. (3), and we obtain

$$n + m = 0, \tag{8}$$

and

$$m = -\frac{d}{\bar{\beta}(1+L\bar{\beta})}. \tag{9}$$

On inserting Eq. (9) into Eq. (8), we get

$$n = \frac{d}{\bar{\beta}(1+L\bar{\beta})}. \tag{10}$$

Therefore, the exact solution of$f(\eta)$ becomes

$$f(\eta) = \frac{d}{\bar{\beta}(1+L\bar{\beta})}(1-e^{-\bar{\beta}\eta}). \tag{11}$$

This solution meets the boundary conditions in Eq. (3) for $\bar{\beta} \succ 0$ which are required for calculating flow and skin friction.
The third- degree algebraic equation shown below is generated by inserting Eq. (11), into Eq. (1).

$$L\overline{\beta}^3+\overline{\beta}^2-ML\left(\frac{\overline{C_1}}{\overline{C_2}}\right)\overline{\beta}-\left(d\overline{C_2}+M\right)\left(\frac{\overline{C_1}}{\overline{C_2}}\right)=0. \tag{12}$$

There is only one positive root for according to Descartes' rule of signs and the fact $\overline{\beta}\succ 0$ which is given by

$$\overline{\beta}=\frac{1}{6L}\left(-2+2^{\frac{2}{3}}\Lambda_1^{\frac{1}{3}}+\frac{2\,2^{\frac{1}{3}}\Lambda_2^{\frac{1}{3}}}{\Lambda_1^{\frac{1}{3}}}\right), \tag{13}$$

where

$$\begin{aligned}\Lambda_1&=-2+27d\,L^2\,\overline{C_1}+18M\,L^2\,\frac{\overline{C}_1}{\overline{C}_2}+\\&\sqrt{4\left(-1-3M\,L^2\,\frac{\overline{C_1}}{\overline{C_2}}\right)^3+\frac{(2\overline{C_2}-9L^2\overline{C_1}(2M+3d\,\overline{C_2}))^2}{\overline{C_2}^2}},\\\Lambda_2&=1+3M\,L^2\,\frac{\overline{C_1}}{\overline{C_2}}.\end{aligned} \tag{14}$$

When there is no slip, Eq. (11) leads to

$$f(\eta)=\frac{1}{\overline{\beta}}(1-e^{-\overline{\beta}\eta}),\ \overline{\beta}=\sqrt{\overline{C_1}+\frac{\overline{C}_1}{\overline{C}_2}M}. \tag{15}$$

This solution is consistent with [29].The exact solution $f(\eta)$ in terms of β is then

$$f(\eta)=\frac{6d\,L\left(1-e^{-\frac{1}{6L}\left(-2+2^{\frac{2}{3}}\Lambda_1^{\frac{1}{3}}+\frac{2\,2^{\frac{1}{3}}\Lambda_2^{\frac{1}{3}}}{\Lambda_1^{\frac{1}{3}}}\right)\eta}\right)}{\left(-2+2^{\frac{2}{3}}\Lambda_1^{\frac{1}{3}}+\frac{2\,2^{\frac{1}{3}}\Lambda_2^{\frac{1}{3}}}{\Lambda_1^{\frac{1}{3}}}\right)+\frac{1}{6}\left(-2+2^{\frac{2}{3}}\Lambda_1^{\frac{1}{3}}+\frac{2\,2^{\frac{1}{3}}\Lambda_2^{\frac{1}{3}}}{\Lambda_1^{\frac{1}{3}}}\right)^2}. \tag{16}$$

Substituting Eq. (11) for Eq. (2) results in:

$$\begin{aligned}&g''(\eta)+\overline{\lambda}_1\,\mathrm{Pr}(n+me^{-\overline{\beta}\eta})g'(\eta)+(2\overline{\lambda}_1\,\mathrm{Pr}\,me^{-\overline{\beta}\eta})g(\eta)=\\&-\overline{\lambda}_2\,\mathrm{Pr}\,Ec(\overline{\beta}^2me^{-\overline{\beta}\eta})^2,\end{aligned} \tag{17}$$

where

$$\overline{\lambda_1}=\frac{k_f}{(1+R)k_{nf}}\overline{C}_3,\overline{\lambda_2}=\frac{k_f}{(1+R)k_{nf}}\frac{\overline{C_3}}{\overline{C_4}}. \tag{18}$$

Eq. (17) is difficult to solve using neither the Laplace transform nor the power series approach due to the inclusion of $e^{-\beta\eta}$ in this equation, as well as the infinite boundary condition Eq (3). Then, using the following independent variable, we must convert Eq. (17) into polynomial type coefficients:

$$\tau = -\overline{\mathrm{Pr}}\, e^{-\bar{\beta}\eta}, \overline{\mathrm{Pr}} = \frac{\mathrm{Pr}}{\bar{\beta}^2}. \tag{19}$$

Taking

$$\varpi = \frac{d}{1+L\bar{\beta}}, \varsigma = 1-\bar{\lambda}_1\, \overline{\mathrm{Pr}}\, \varpi, \delta = \frac{\overline{\lambda_2} Ec}{\overline{\mathrm{Pr}}} \varpi^2\, \bar{\beta}^2. \tag{20}$$

Eq. (17) becomes

$$\tau\, g''(\tau) + (\varsigma - \bar{\lambda}_1 \varpi\ \tau)\, g'(\tau) + 2\bar{\lambda}_1 \varpi\, g(\tau) = -\delta\, \tau. \tag{21}$$

With the transformed boundary conditions

$$g(-\overline{\mathrm{Pr}}) = 1,\ g(0) = 0. \tag{22}$$

Then the exact solution of the temperature function in terms of η is

$$\begin{aligned} g(\eta) = {} & (1-\gamma_0(-\overline{\mathrm{Pr}})^2)\frac{M[-1-\varsigma, 2-\varsigma, (\varsigma-1)e^{-\bar{\beta}\eta}]}{M[-1-\varsigma, 2-\varsigma, \varsigma-1]} e^{-\bar{\beta}(1-\varsigma)\eta} \\ & +\gamma_0(-\overline{\mathrm{Pr}})^2 (e^{-\bar{\beta}\eta})^2, \end{aligned} \tag{23}$$

where $M[p, q, \bar{y}] = \sum_{s=0}^{\infty} \frac{p(p+1)....(p+s-1)}{q(q+1)....(q+s-1)} \frac{\bar{y}}{s!}$ is Kummer's function [33], and $\gamma_0 = -\frac{\delta}{2(1+\varsigma))}$.

When L=R=0 and d = 1, the solution provided by Eq. (23) simplifies to the one given in Ref. [29] (Eq. (36)). Furthermore, the present exact solutions may be easily checked by immediately substituting them into the original differential equations.

3. Results and Discussion

Because of their extraordinary flow stability, carbon nanotubes have lately advanced. For various values of the controlling *L, R, M, Pr, ϕ,*and*Ec* parameters, Eqs. (1) and (2) applied to the boundary conditions Eq. (3) have been solved analytically [29]. Tables 2-4 provide the numerical results of the local skin friction $-f''(0)$ and the local Nusselt number $-g'(0)$. Figs. 1–22 show the behavior of dimensionless similarity function, streamline contours, velocity, sheer stress, temperature, and local Nusselt number profiles in the stretched sheet scenario.

3.1. Numerical Results for $-f''(0)$ and $-g'(0)$

Table 2 compares the proposed study's results for the local Nusselt number $-g'(0)$ at various Prandtl numbers to those discovered in refs. [29, 34]. The discovery proved that the Pr values are completely correlated. It is worth noting that $-g'(0)$is an increasing function. Furthermore, as shown in Table 3, the numerical values of the local skin friction $-f''(0)$ for each of Cu-water, Ag-water, SWCNT, and MWCNT in the absence of slip and radiation parameters at various values of M and ϕ are perfectly in agreement with those reported in references [29, 35]. The numerical findings reveal that in the absence of a magnetic field, at M=0, the skin friction coefficient for Cu-water and Ag-water nanofluids rises with increasing solid volume fraction [32]. Table 4 illustrates the variation in numerical results of $-f''(0)$ and $-g'(0)$ for each of Cu-water, Ag-water, SWCNT, and MWCNT at different values of L, R, M, and ϕ when Ec=0.1, and Pr=6.7850 in the current study.

Table 2 Comparison of numerical results for $-g'(0)$ at different values of Prandtl numbers in the present study with those obtained in Refs. [29, 34]

Pr	Ref. [29]	Ref. [34]	Present results
0.72	1.08852	1.0885	1.088524024
1.0	1.33333	1.3333	1.333333333
3.0	2.50973	2.5097	2.509725227
10.0	4.79687	4.7969	4.796873283
100.0	15.71163	15.7120	15.71196715

It is deduced that $-f''(0)$ is a monotonic function with regard to Cu-water and Ag-water, but a decreasing function with respect to SWCNT and MWCNT by increasing the L, R, and M parameters. $-g'(0)$ on the other hand, is a declining function for all nanofluids.

3.2. Flow and Heat Transfer Facts and interpretations

Figs. 1 and 2 provide plots of variation of dimensionless similarity functions$f(\eta)$ and$g(\eta)$ at the specified data in the current study and earlier published work [29]. It is important to note that in the absence of slip, i.e., L=0,the profile of $f(\eta)$ as shown in Fig. 1 for the MWCNT is greater than for the SWCNT, Cu-water, and Ag-water, whereas the temperature profiles of $g(\eta)$ in Fig. 2 for the SWCNT are the highest. Furthermore, as the values of the slip parameter increase, the dimensionless similarity functions $f(\eta)$ for each of MWCNT, SWCNT, Cu-water, and Ag-water decrease, but vice versa for the temperature profiles $g(\eta)$ as the values of the solid volume fraction increase. Figs. 3-5 depict heat transmission inside the boundary layer region using streamline contours of MWCNT, SWCNT, Cu-water, and Ag-water. These graphsare presented for three distinct values of L: (a) L=0.0, (b) L=0.5, and (c) L=1 with the other parameters set to M=0.01, ϕ=0.25, Ec=0.1, and d=1. Again, L=0.0 depicts the merely stretching situation, whereas $L\neq0.0$ indicates the moving case. When L is increased from 0 to 1, these motions become more pronounced within the boundary layer area. As a result, with larger values of L, the streamlines transport more energy during the fluid flow; hence, L plays an important role in the formation of the boundary layer flow area (see Figs. 9 and 10).

Table 3 Comparison of numerical results for $-f''(0)$ in the absence of slip and radiation parameters at various values of M and ϕ in the present study with those obtained in Refs. [29, 35]

		Ref. [29]		Ref. [35]	
M	ϕ	Cu-water	Ag-water	Cu-water	Ag-water
0	0.05	1.108919904	1.139659703	1.10892	1.13966
	0.1	1.174746021	1.225068143	1.17475	1.22507
	0.15	1.208862320	1.272152949	1.20886	1.27215
	0.2	1.218043809	1.289788016	1.21804	1.28979
2	0.05	1.728872387	1.74874830	1.72887	1.74875
	0.1	1.707892022	1.742888091	1.70789	1.74289
	0.15	1.671398302	1.717730276	1.67140	1.71773
	0.2	1.621264175	1.675834100	1.62126	1.67583
			Present Results		
M	ϕ	Cu-water	Ag-water	SWCNT	MWCNT
0	0.05	1.108919904	1.139659703	0.974860316	0.951967598
	0.1	1.174746021	1.225068143	0.944438410	0.902716495
	0.15	1.208862320	1.272152949	0.909249444	0.852365612
	0.2	1.218043809	1.289788016	0.869757340	0.801035688
2	0.05	1.728872387	1.748748300	1.646101156	1.632647753
	0.1	1.707892022	1.742888091	1.558470678	1.533546221
	0.15	1.671398302	1.717730276	1.469339554	1.434834942
	0.2	1.621264175	1.675834099	1.378892540	1.336609508

The findings shown in Fig. 6 regarding the influence of the slip parameter L on velocity variation show that $f'(\eta)$ is a decreasing function in L. Furthermore, the MWCNT-nanofluids have faster velocities than the SWCNT-nanofluids, which is consistent with the results of Fig. 8 and the other nanoparticles (Cu-water and Ag-water) as shown in Fig. 7. In contrast, as seen in Figs. 6 and 7, increasing the slip parameter L causes the shear stress $f''(\eta)$ to increase. Physically, It can be shown that as L grows, the wall slips velocity drops while the wall drag force increases. For a larger value of L and a short flow passes into the nanofluid, the nanofluid velocity is slowed down off quickly. The flow can penetrate relatively deeply for a modest value of L. The shear stress profiles at the wall are larger for a large value of L, and they grow fast as the flow enters into the nanofluid. It is worth noting that in Figs. 6 and 7, the concavity of the velocity $f'(\eta)$ and the shear stress $f''(\eta)$ profiles is shifted from above to down.

Table 4 Variations of numerical results for $-f''(0)$ and $-g'(0)$ at various values of L, R, M, and ϕ when Ec=0.1 and Pr=6 .7850 in the present study

						$-f''(0)$	
L	R	M	ϕ	Cu-water	Ag-water	SWCNT	MWCNT
1	1	0	0.05	0.451038219	0.456562203	0.425025631	0.420238679
			0.1	0.462685934	0.471149914	0.418640297	0.409558845
			0.15	0.468463835	0.478749835	0.411006550	0.398063307
			0.2	0.469990180	0.481520936	0.402103162	0.385687651
3	5	0.1	0.05	0.225492740	0.226771004	0.219455243	0.218342243
			0.1	0.227585942	0.229577545	0.217118779	0.214945178
			0.15	0.228412363	0.230869212	0.214443019	0.211251204
			0.2	0.228488915	0.231085016	0.211398287	0.207222484
5	10	0.5	0.05	0.160958245	0.161226725	0.159772323	0.159568261
			0.1	0.160424833	0.160905202	0.158140630	0.157716259
			0.15	0.159686464	0.160343847	0.156358478	0.155695813
			0.2	0.158745002	0.159557384	0.154403462	0.15348256
						$-g'(0)$	
L	R	M	ϕ	Cu-water	Ag-water	SWCNT	MWCNT
1	1	0	0.05	1.783121169	1.755546964	1.380374490	1.428477746
			0.1	1.604982420	1.559269414	1.065252751	1.125818696
			0.15	1.457837201	1.398823398	0.865564763	0.930729013
			0.2	1.333340229	1.264003676	0.724175740	0.791012026
3	5	0.1	0.05	0.704628283	0.690377389	0.530640248	0.553698212
			0.1	0.625380551	0.601905211	0.395335561	0.424797834
			0.15	0.561570699	0.531598949	0.312361843	0.344182003
			0.2	0.509181816	0.474419170	0.255741049	0.288305237
5	10	0.5	0.05	0.294329004	0.288338153	0.199582973	0.209512817
			0.1	0.266266609	0.255860920	0.143272409	0.154802619
			0.15	0.243312656	0.229537559	0.111623322	0.123323245
			0.2	0.224350296	0.207919858	0.091324210	0.102865153

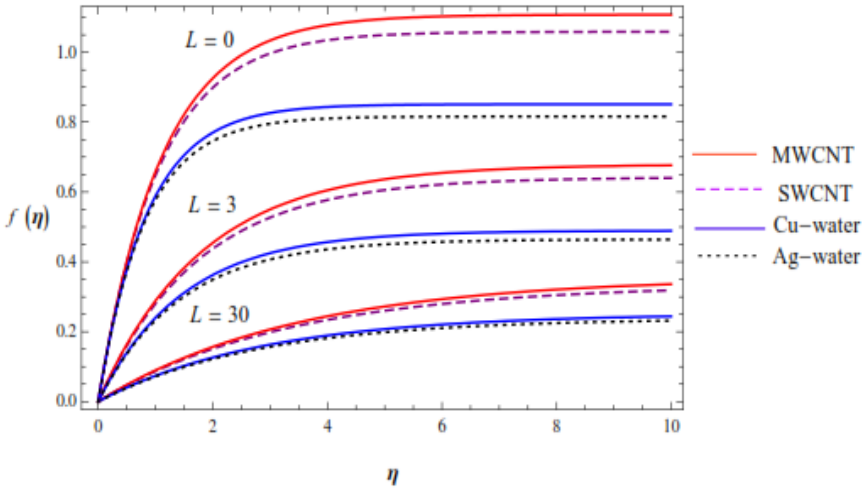

Fig. 1 Plots of the dimensionless stream functions for MWCNT and SWCNT in this study and prior published work [29] at different values of slip parameter when M=R=0, Ec= ϕ=0.1, and d=1

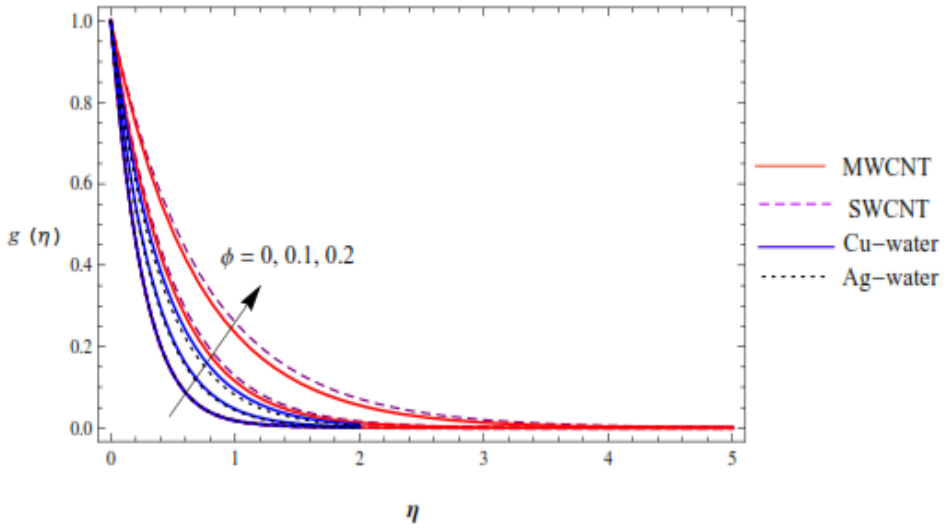

Fig. 2 Plots of the temperature profiles of MWCNT and SWCNT in this study and prior published work [29] at different values of solid volume fraction when M=R=0, Ec=0.1, and d=1

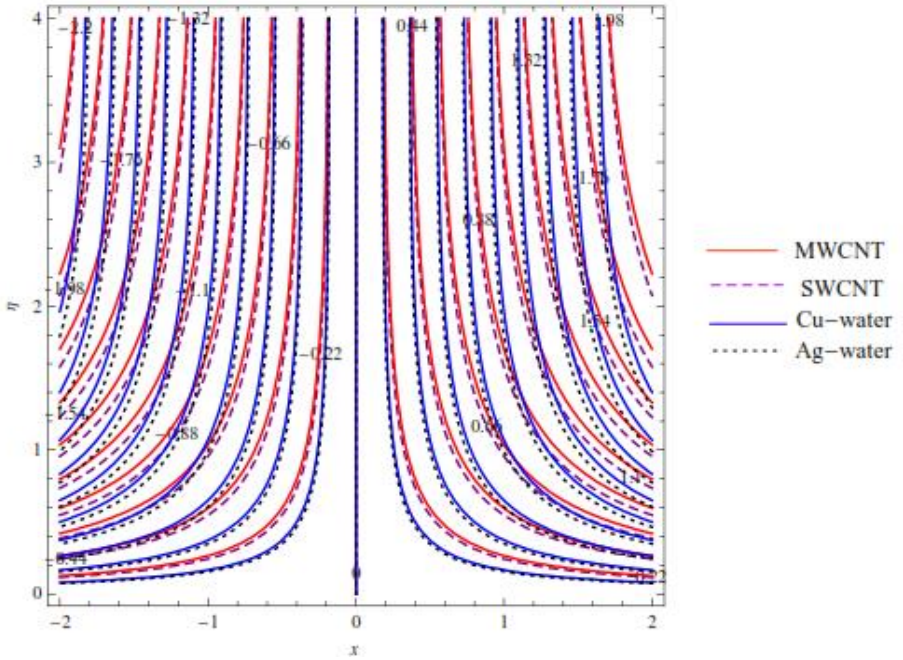

Fig. 3 Streamline contours at L=0, M=0.01, ϕ=0.25, Ec=0.1, and d=1

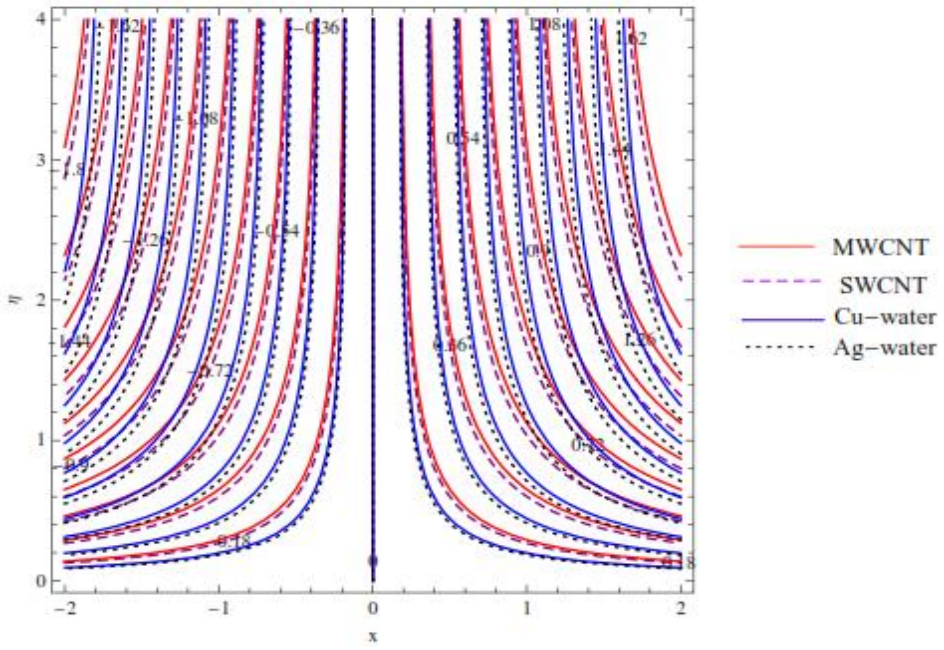

Fig. 4 Streamline contours at L=0.5, M=0.01, ϕ=0.25, Ec=0.1, and d=1

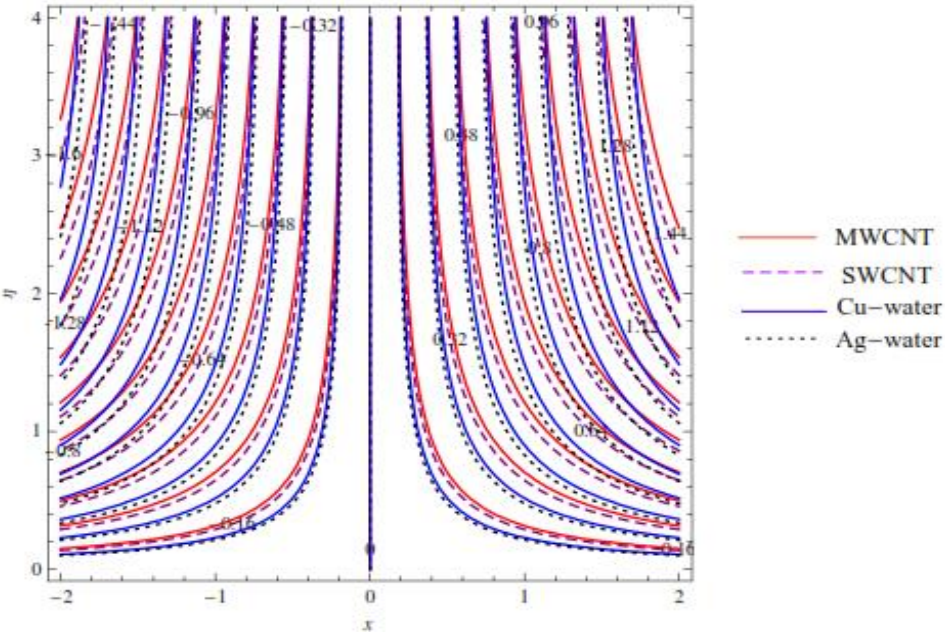

Fig. 5 Streamline contours at L=1, M=0.01, ϕ=0.25, Ec=0.1, and d=1

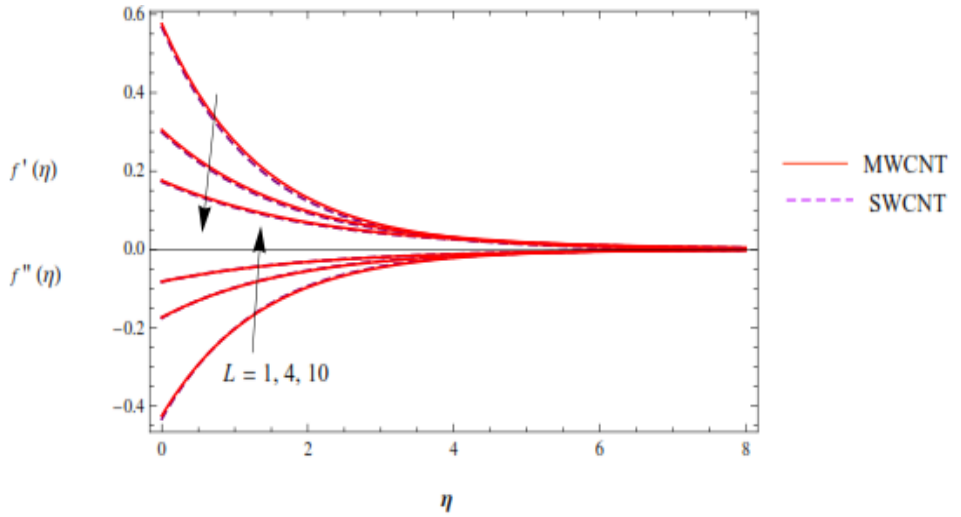

Fig. 6 Impact of the slip parameter on the velocity and the shear stress profiles for MWCNT and SWCNT at M= Ec= ϕ=0.1, R=5, and d=1

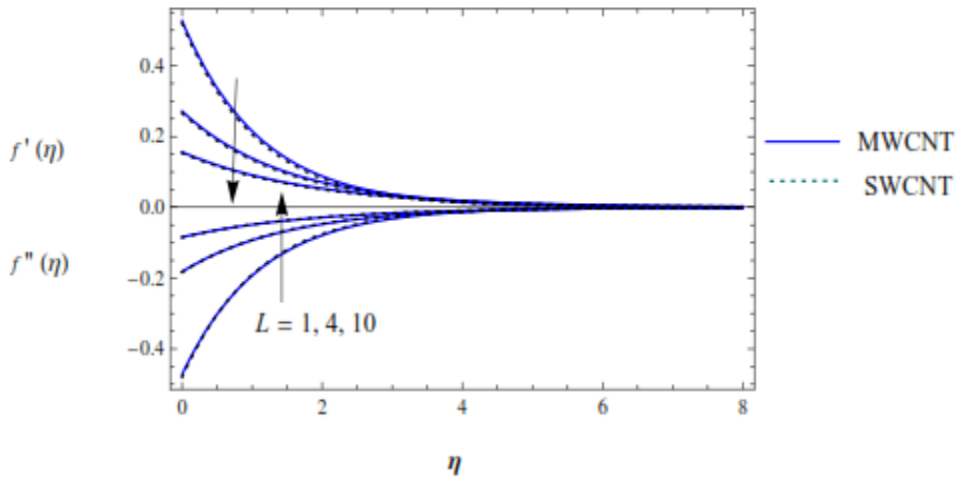

Fig. 7 Impact of the slip parameter on the velocity and the shear stress profiles for MWCNT and SWCNT at M= Ec= ϕ=0.1, R=5, and d=1

Because of the importance of this discovery for engineers and researchers in practically every aspect of physics and engineering, several real-world examples are offered to support the stated modelling findings. Nuclear power plants, gas turbines, and various propulsion technologies for aeroplanes, missiles, satellites, and space vehicles are examples of such technical specialties'. Figs. 8-10 show the impacts of the solid volume fraction parameter on the

velocity and temperature profiles of SWCNT and MWCNT suspended nanofluids, which are compared to those obtained in [29].

Fig. 8 demonstrates that increasing the solid volume fraction of SWCNT and MWCNT nanofluids enhances fluid velocity, but increasing the solid volume fraction of Cu-water and Ag-water reduces fluid velocity [29]. Fig. 8 further shows that MWCNT suspension nanofluids have greater velocities than all the other nanofluids, which may be advantageous in both medical and industrial aspects. The increase in temperature with the addition of additional nanoparticles to the base fluids has been a good result in the field of nanofluids. This is due to an increase in the thermophysical properties of the fluid.

As shown in Figs. 9 and 10, this conclusion is likewise validated for CNTs. Furthermore, Figs. 9 and 10 reveal that SWCNT nanofluids have a greater temperature than MWCNT nanofluids [36]. Additionally, Figs. 9 and 10 show that increasing L (L=0, 1) improves the temperature profiles of all nanofluids. Figs. 11 and 12 show temperature profiles for SWCNT, MWCNT, Cu-water, and Ag-water suspended nanofluids at different values of three parameters, Pr, M, and L when R=3, Ec=ϕ=0.1, and d=1. Physically, it is known that temperature profiles decline at large Prandtl numbers Pr, as seen in Figs. 11 and 12 [37].

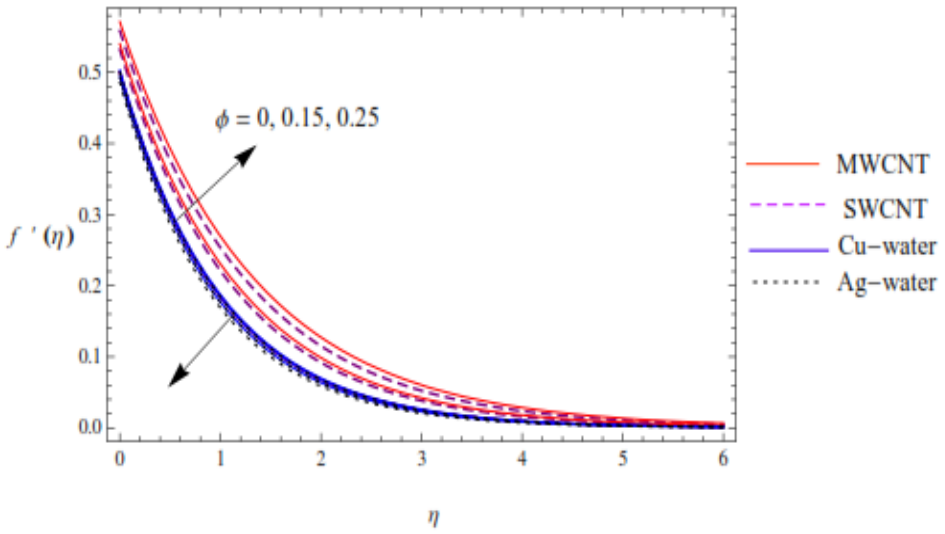

Fig. 8 Impact of the solid volume fraction on the velocity profiles at L=1, M=0.5, R=3, Ec=0.1, and d=1

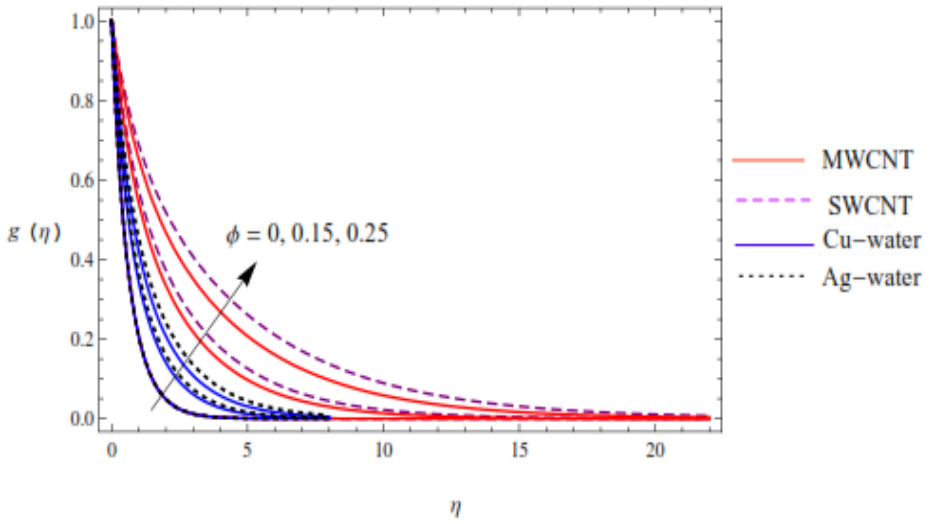

Fig. 9 Impact of the solid volume fraction on the temperature profiles at L =0, M=0.5, R=3, Ec=0.1, and d=1

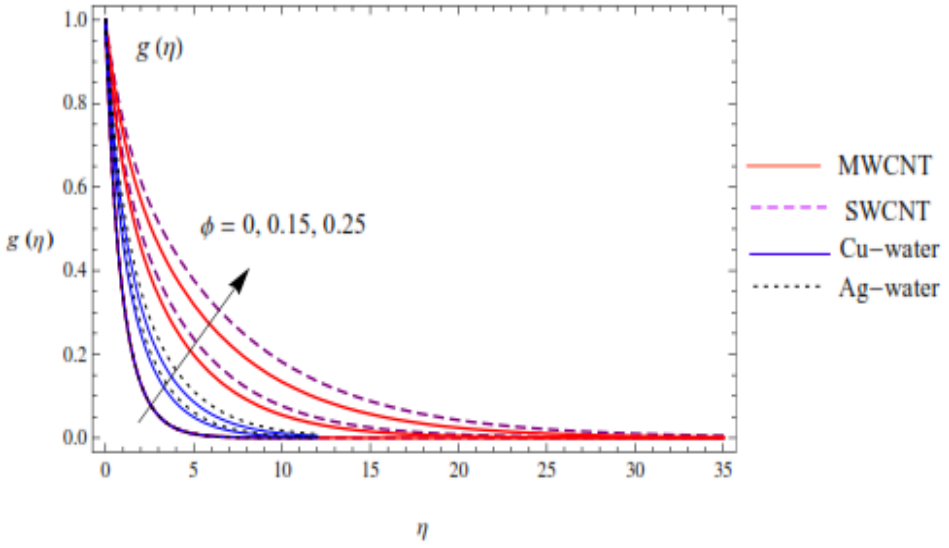

Fig. 10 Impact of the solid volume fraction on the temperature profiles at L=1, M=0.5, R=3, Ec=0.1, and d=1

This is consistent with the physical reality that the thickness of the thermal boundary layer decreases as Pr increases. In other words, increasing the value of Pr accelerates the decay of the temperature field away from the heated surface, increasing the rate of heat transfer and a

decrease in the thickness of the thermal boundary layer [38]. However, when the magnetic and slip factors are coupled, the temperature profiles grow as the magnetic and slip values increase.

Figs. 11 and 12 show temperature profiles for various values of the M and L parameters, as well as the Prandtl number, in the presence of SWCNT, MWCNT, Cu-water, and Ag-water nanoparticles. The uniform thermal radiation [32] clearly shows that in the four examples listed above, the heat of water-based SWCNT, MWCNT, Cu-water, and Ag-water accelerates with increasing magnetization, implying that the external electric field tends to heat the fluid and improves thermal performance from the surface. Cos of the composite members' electric and thermal conductivity of SWCNT-water and MWCNT–water, the dynamism and thermal boundary layer thickness of SWCNT–water and MWCNT–water are significantly greater than those of Cu-water and Ag-water. It shows that reducing the density of the water-based SWCNT, MWCNT elevates the fluid temperature difference and proves that applying magnetism to an electrically conducting fluid provides a skid steer strength that induces acceleration in the nanofluid temperature [16]. Furthermore, it is discovered that the action of viscous heating causes a rise in temperature, which is more prominent in the presence of a magnetic field.

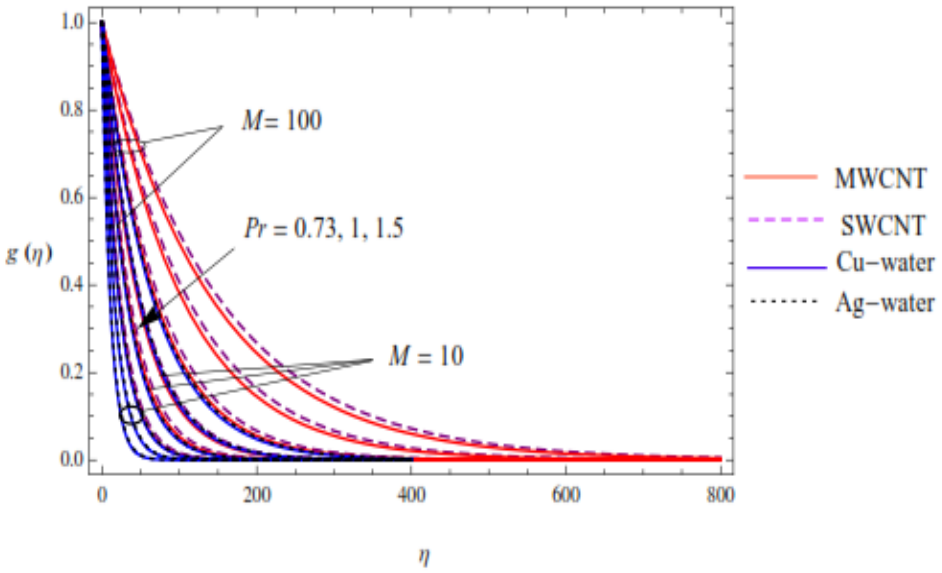

Fig. 11 Impact of Prandtl number and magnetic parameter on the temperature profiles at L=0, R=3, Ec=ϕ=0.1, and d=1

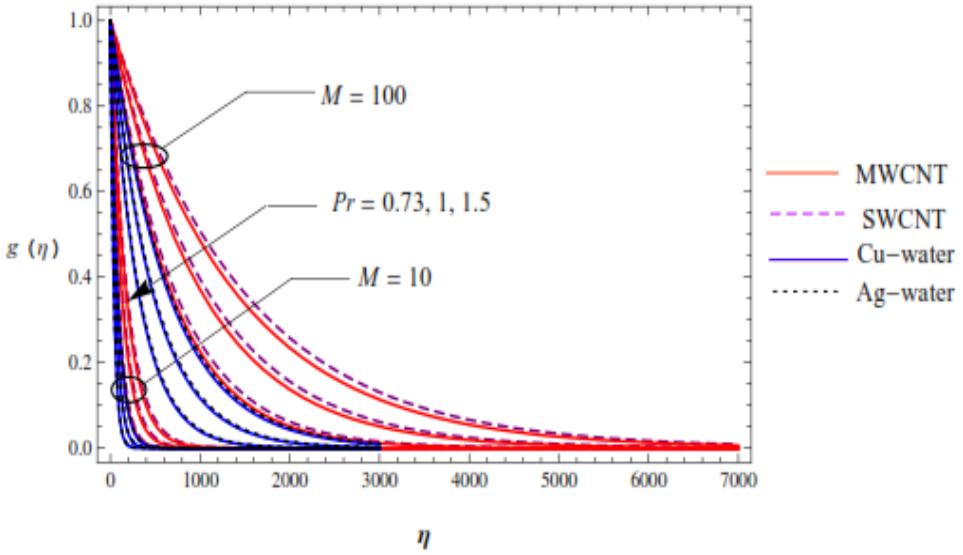

Fig. 12 Impact of Prandtl number and magnetic parameter on the temperature profiles at L=1, R=3, Ec=ϕ=0.1, and d=1

Figs. 13-15 in this chapter depict the physical effects of several parameters on the solution property. It is worth mentioning that in the presence of the radiation parameter, raising the emission parameter improves the amount of radiative heat transmitted to SWCNT-water, MWCNT-water, and thus the fluid temperature substantially when contrasted toCu-water and Ag-water.

Figs. 16 and 17 depict the effect of the M and Ec parameters on the heat transport $-g'(\eta)$ curves of SWCNT, MWCNT, Cu-water, and Ag-water nanofluids. Physically, as demonstrated in Figs. 11 and 12, raising the M parameter enhances the temperature profiles of all the aforesaid nanofluids while decreasing the heat transfer $-g'(\eta)$ profiles, as illustrated in Figs. 16 and 17 [38]. Furthermore, by raising the Eckert number, the heat transfer $-g'(\eta)$ profiles for these nanofluids become rather deep. The heat transfer $-g'(\eta)$ profiles for Cu-water are found to be greater than those for Ag-water, MWCNT, and SWCNT nanofluids at all M parameter values. Figs. 16 and 17 show that as M increases, the heat transmission $-g'(\eta)$ profiles decrease and the thermal boundary layer thickens. Furthermore, for high Ec values, the heat transfer $-g'(\eta)$ profiles of MWCNT and SWCNT reduce fast.

Figs. 18-20 indicate the effectiveness of various parameters, R and Pr, on the heat transfer $-g'(\eta)$ graphs of SWCNT, MWCNT, Cu-water, and Ag-water nanofluids. It was discovered that the heat transfer $-g'(\eta)$ profiles for Cu-water are larger than those of other nanofluids at all R parameter values. Figs. 18-20 indicate that when R grows, the heat transmission $-g'(\eta)$ profiles of Cu-water and Ag-water drop and the thermal boundary layer deepens in comparison to MWCNT and SWCNT nanofluids. Additionally, at high Pr values, the Cu-water and Ag-water heat transfer $-g'(\eta)$ profiles advance quicker than the MWCNTand SWCNT nanofluids. This is significant in thermal engineering, mechanics, and science, such as thermal processing, airflow, and conditioning systems, as well as renewable energies.

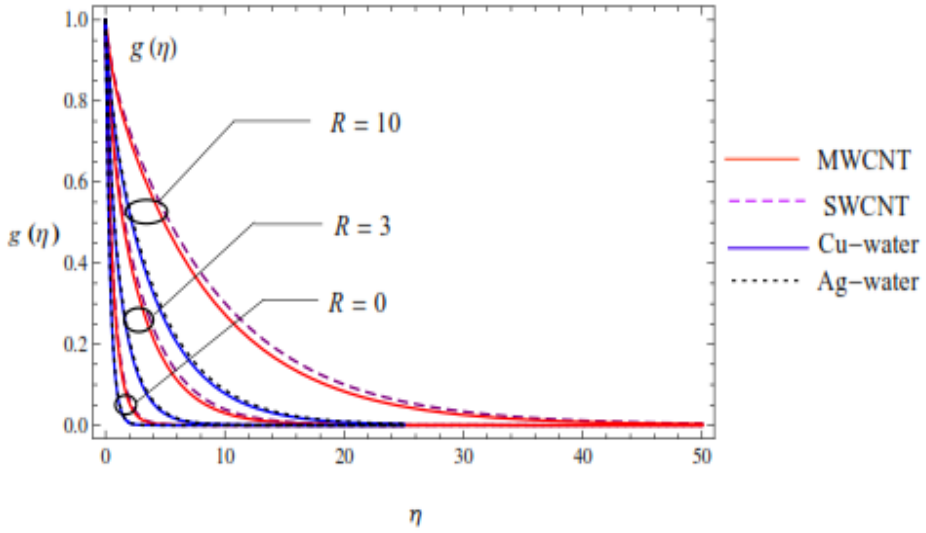

Fig. 13 Impact of radiation parameter on the temperature profiles at L=0, M=0.5, Ec= ϕ=0.1, and d=1

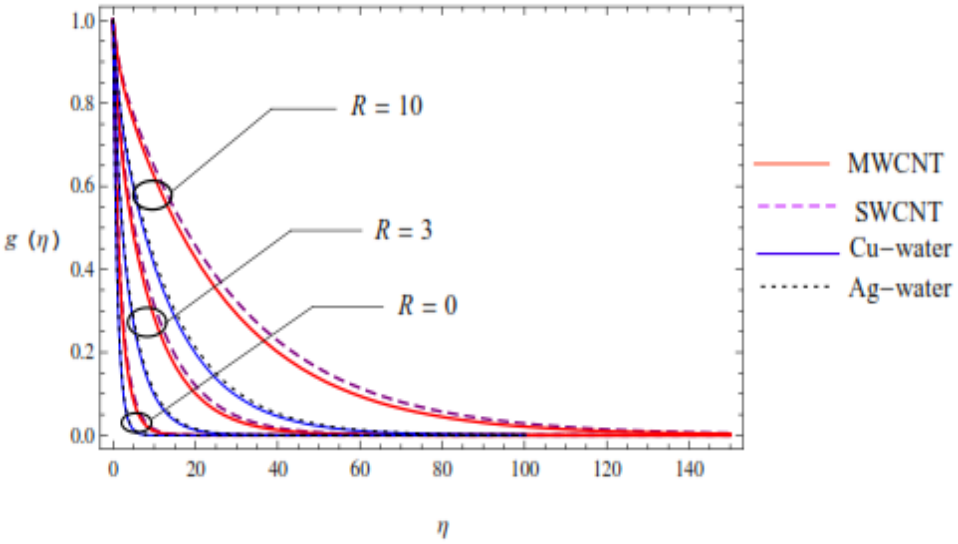

Fig. 14 Impact of radiation parameter on the temperature profiles at L=10, M=0.5, Ec= ϕ=0.1, and d=1

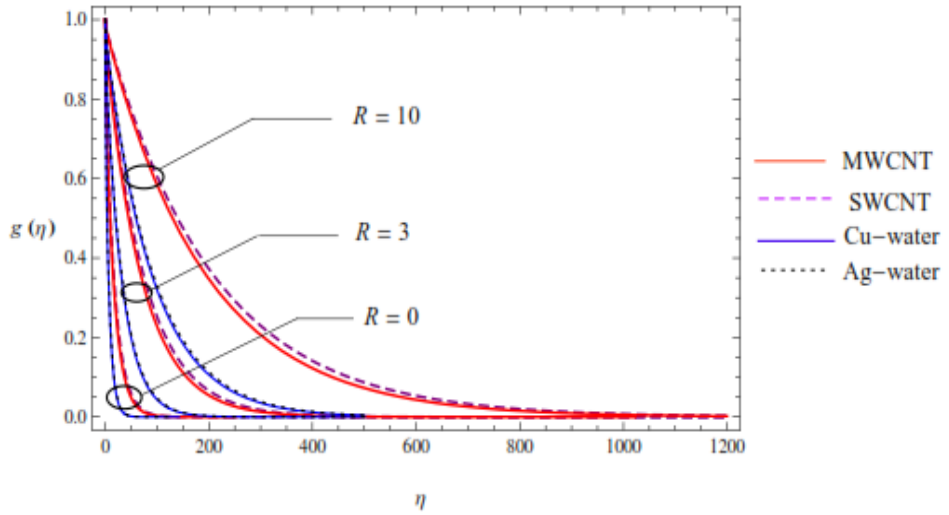

Fig. 15 Impact of radiation parameter on the temperature profiles at L=100, M=0.5, Ec= ϕ=0.1, and d=1

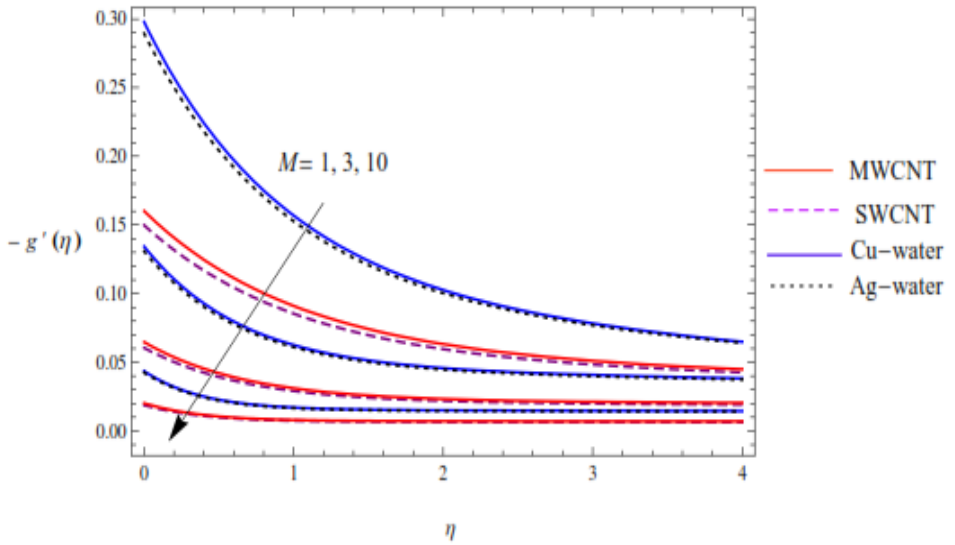

Fig. 16 Impact of magnetic parameter on the heat transfer rate profiles at Ec=1, L=10, R=3, ϕ=0.1, and d=1

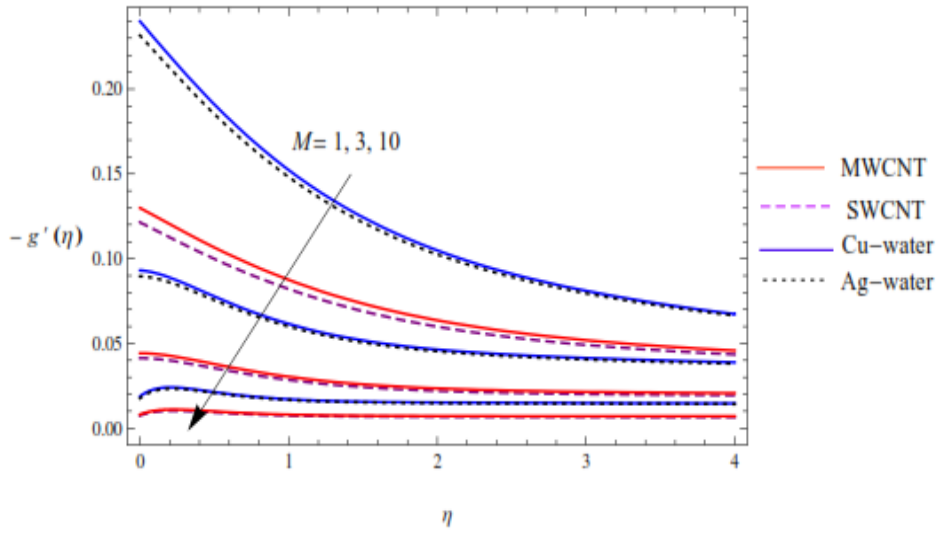

Fig. 17 Impact of magnetic parameter on the heat transfer rate profiles at Ec=10, L=10, R=3, ϕ=0.1, and d=1

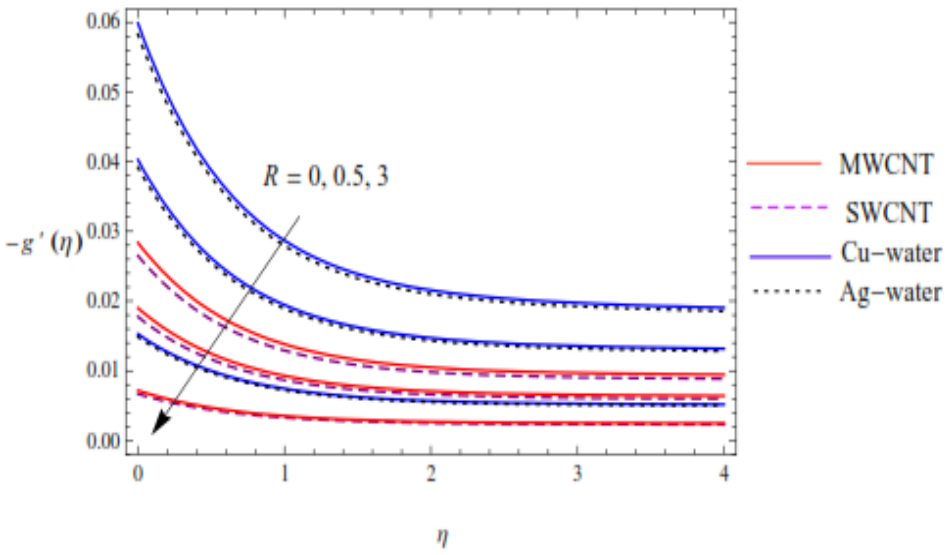

Fig. 18 Impact of radiation parameter on the heat transfer rate profiles at Pr=0.73, L=10, Ec =1, ϕ=0.1, and d=1

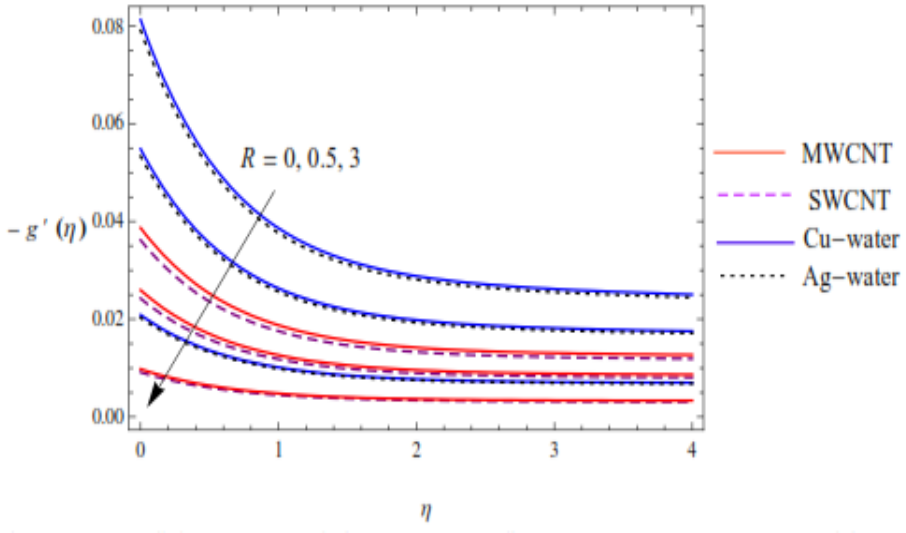

Fig. 19 Impact of radiation parameter on the heat transfer rate profiles at Pr=1, L=10, Ec =1, ϕ=0.1, and d=1

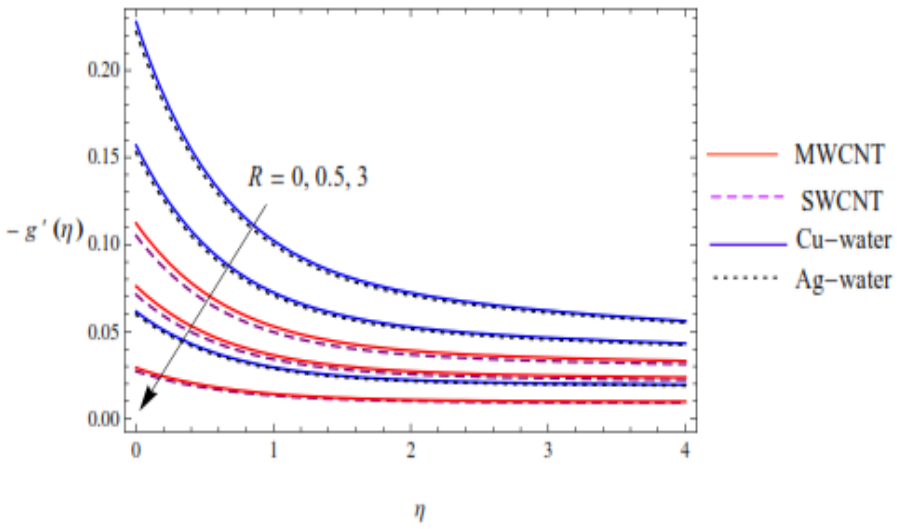

Fig. 20 Impact of radiation parameter on the heat transfer rate profiles at Pr=3, L=10, Ec =1, ϕ=0.1, and d=1

Finally, Figs. 21 and 22 depict the heat transfer $-g'(\eta)$ profiles of SWCNT, MWCNT, Cu-water, and Ag-water nanofluids at various values of L and ϕ parameters.

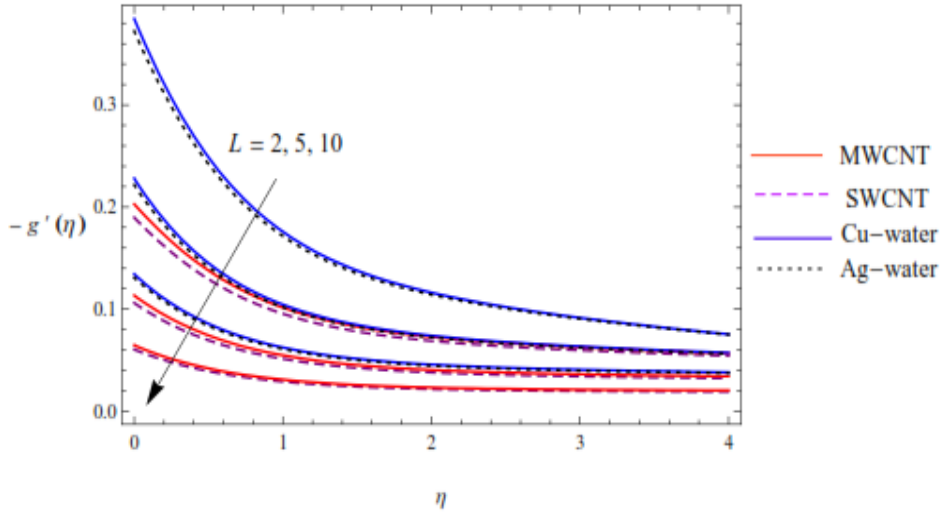

Fig. 21 Impact of the slip parameter on the heat transfer rate profiles at ϕ=0.1, M=R=3, and Ec= d=1

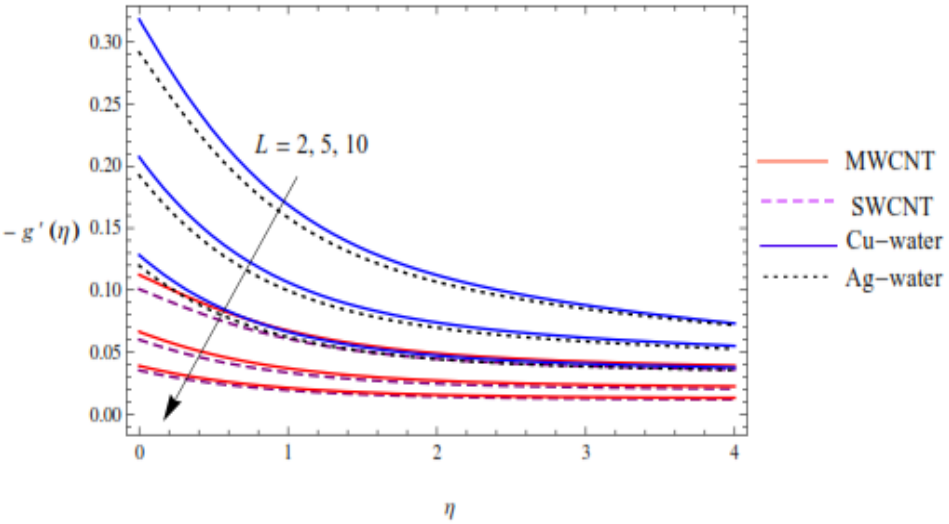

Fig. 22 Impact of the slip parameter on the heat transfer rate profiles at ϕ=0.25, M=R=3, and Ec= d=1

The profiles of heat transfer $-g'(\eta)$ of SWCNT, MWCNT, Cu-water, and Ag-water nanofluids decrease as L and ϕ parameters rise. It has been shown that all of these nanofluids are faster decrease when the solid volume fraction is greater. The thickness of the thermal boundary layer profiles of the heat transfer $-g'(\eta)$ of MWCNT and SWCNT is lower than that of Cu-water and Ag-water nanofluids as the thickness of the thermal boundary layer profiles increases.

4. CONCLUSIONS

The effects of radiation on the flow of carbon nanotube suspended nanofluids across a stretched sheet influenced by slip state in the presence of a magnetic field, as well as their applications in medicine and engineering, were investigated. Carbon nanotubes may be used for a variety of purposes, including thermal conductivity control, field emission, conductive properties, energy storage, CNT-based molecular electronics, and thermal materials. Cos of their large molecular mass, they are nearly impermeable in all known solutions. Some of the applications of interest that involve heat transfer via natural convection include the design of chemical processing equipment, the design of boilers, temperature and moisture ranges over agricultural areas, and thermal safety systems. Analytical solutions were found for a system of nonlinear ordinary differential equations with specific physical parameter values of L, M, R, Ec,ϕ, and Pr. Our analyses revealed the following significant discoveries:

At varying values for the L, R, and M parameters, it was revealed that $-f''(0)$ is a monotonic function in terms of Cu-water and Ag-water, but a decreasing function in terms of SWCNT and MWCNT, whereas $-g'(0)$ is a decreasing function applicable to all nanofluids.

Temperature profiles were discovered to be extremely respectful provided to the solid volume fraction, magnetic, slip, and radiation parameters. So, SWCNT nanofluids have a greater temperature than MWCNT, Ag, and Cu nanofluids (see Figs. 9 and 10, Figs. 11 and 12, and Figs. 13 and 14) when these three parameters increase. However, the MWCNT nanofluids had a greater stream function, streamlines, and velocity profiles than the SWCNT, Cu-water, and Ag-water nanofluids (see Figs. 1 and 2, Figs. 4 and 5, Figs. 6 and 7, and Fig. 8) in the case of the increase of the slip parameter. The solid volume fraction, magnetic, slip, and radiation characteristics all improve the temperature field and raise the thickness of the thermal function's boundary layer in the case of a stretched sheet, but they reduce the heat transfer rates of all other nanofluids. It is also concluded that when the slip parameter increases, the heat transfer profiles $-g'(\eta)$ for Cu-water grow larger than those for the other nanofluids (see Figs. 21 and 22). Because of its numerous uses in chemical manufacturing engineering, this partial slip boundary condition has received a lot of attention.

The velocity profiles of the SWCNT and MWCNT nanofluids increase as the solid volume fraction increases, whereas the reverse is true for the Cu-water and Ag-water nanofluids (see Fig. 8). Furthermore, as the ϕ parameter is raised, the MWCNT and SWCNT heat transfer rates are deeper than the Cu-water and Ag-water nanofluids.

As the Prandtl number increases, the temperature profiles of Cu-water, Ag-water, MWCNT, and SWCNT nanofluids decrease while heat transfer rates increase.

The heat transfer profiles $-g'(\eta)$ for Cu-water, Ag-water, MWCNT, and SWCNT nanofluids gradually deepen as the Eckert number increases.

The findings have applications in a variety of fields, including thermo-mechanical processes, biomedical, and the optimal heat transfer structure for a renewable power collecting.

REFERENCES

1. Ajayan, P.M., 1999, *Nanotubes from carbon*,Chem. Rev., 99, pp. 1787-1799**.**
2. Yu, M.F., Files, B.S., Arepalli, S., Ruoff, R.S., 2000, *Tensile loading of ropes of single wall carbon nanotubes and their mechanical properties*, Phys. Rev. Lett., 84, pp. 5552-5555.
3. Otsubo, Y., Fujiwara, M., Kouno, M., Edamura, K., 2007, *Shear-thickening flow of suspensions of carbon nanofibers in aqueous PVA solutions*,Rheol. Acta, 46, pp. 905-912.
4. Dresselhaus, M.S., Dresselhaus, G.P., 2001, *Avouris (Eds.)*,*Carbon Nanotubes*: *Synthesis, Structure, Properties and Applications*, Springer, New York, USA.
5. Harris, P.J., 2001, *Carbon Nanotubes and Related Structures: New Materials for the 21st Century*, University Press, Cambridge,doi: 10.1017/CBO9780511605819.
6. Yanping, Du., Tao, Zhou., Changying, Zhao., Yulong, D., 2022, *Molecular dynamics simulation on thermal enhancement for carbon nano tubes (CNTs) based phase change materials (PCMs),* International Journal of Heat and Mass Transfer, 182, 122017.
7. Zuo, Y.-T., Liu, H.-J., 2021, *Fractal approach to mechanical and electrical properties of graphene/sic composites*, FactaUniversitatis-Series Mechanical Engineering, 19(2), pp. 271-284.
8. Trojanowicz, M., 2006, *Analytical applications of carbon nanotubes: a review*, Trends in Analytical Chemistry, 25, pp. 40-489.
9. Ki-Jung, P., Dongsoo, J., 2007, *Enhancement of nucleate boiling heat transfer using carbon nanotubes*, International Journal of Heat and Mass Transfer, 50, pp. 4499-4502.
10. Murshed, S.M.S., Leong, K.C., Yang, C., 2008, *Thermo physical and electro kinetic properties of nanofluids-a critical review*, Appl. Therm. Eng., 28, pp. 2109-2125.
11. Biercuk, M.J., Llaguno, M.C., Radosavljevic, M., Hyun, J.K., Johnson, A.T., 2002, *Carbon nanotube composites for thermal management*, Appl. Phys. Lett., 80, pp. 2767-2769.
12. Xue, Q., 2005, *Model for thermal conductivity of carbon nanotube based composites*, Phys. B Condens. Matter, 368, pp. 302-307.
13. Schnorr, J.M., Swager, T.M., 2001, *Emerging Applications of Carbon Nanotubes*, Chem. Mater., 23, pp. 646-657.
14. Walvekar, R., Faris, I.A., Khalid, M., 2012, *Thermal conductivity of carbon nanotube nanofluid-experimental and theoretical study*, Heat Transf. Asian Res., 41, pp. 145-163.
15. Khan,W., Khan, Z., Rahi, M., 2014, *Fluid flow and heat transfer of carbon nanotubes along a flat plate with Navier slip boundary*, Appl. Nanosci., 4, pp. 633-641.
16. Kandasamy, R., Muhaimin, I., Mohammad, R., 2016, *Single walled carbon nanotubes on MHD unsteady flow over a porous wedge with thermal radiation with variable stream conditions*, *Alex. Eng. J.,* 55, pp. 275-285.
17. Murshed, S.M., Nieto de Castro, C.A., Lourenço, M.J.V., Lopes, M.L.M., Santos, F.J.V., 2011, *A review of boiling and convective heat transfer with nanofluids*, Renew. Sustain. Energy Rev.,15, pp. 2342-2354.
18. Akbar, N.S., Nadeem, S., Khan, Z.H., 2014, *Thermal and velocity slip effects on the MHD peristaltic flow with carbon nanotubes in an asymmetric channel: application of radiation therapy*, Appl. Nanosci., 4, pp. 849–857.
19. Halelfadla, S., Estellé, P., Aladag, B., Doner, N., Maré, T., 2013, *Viscosity of carbon nanotubes water-based nanofluids: influence of concentration and temperature*, Int. J. Therm. Sci., 71, pp. 111-117.
20. Akbar, N.S., 2015, *Heat transfer and carbon nano tubes analysis for the peristaltic flow in a diverging tube*,Meccanica, 50, pp. 39-47.
21. Khan, M.S., Mei, S., Shabnam, Fernandez-Gamiz, U., Noeiaghdam, S., Shah, S.A., Khan, A., 2022, *Numerical analysis of unsteady hybrid nanofluid flow comprising CNTs-Ferrousoxide/water with variable magnetic field*, Nanomaterial,12, 180.
22. Ding, Y., Alias, H., Wen, D., Williams, R.A., 2006, *Heat transfer of aqueous suspensions of carbon nanotubes (CNT nanofluids)*,Int. J. Heat Mass Transf., 49, pp. 240–250.
23. He, J.-H., Abd Elazem, N.Y., 2021, *Insights into partial slips and temperature jumps of a nanofluid flow over a stretched or shrinking surface*, Energies, 14, 6691.

24. Abd Elazem, N.Y., Elgazery, N.S., 2021, *Unsteady radiative nanofluid flow near a vertical heated wavy surface with temperature-dependent viscosity*, Chinese Journal of Physics, 74, pp. 38–52.
25. Zainal, N.A., Nazar, R., Naganthran, K., Pop, I., 2020, *Unsteady Three-Dimensional MHD Non-Axisymmetric Homann Stagnation Point Flow of a Hybrid Nanofluid with Stability Analysis*, Mathematics, 8, 784, doi: 10.3390/math8050784.
26. Suganya, S., Muthtamilselvan, M., Abdalla, B., 2021, *Effects of radiation and chemical reaction on Cu-Al2O3/water hybrid flow past a melting surface in the existence of cross magnetic field*, *Ricerche di Matematica*, doi: 10.1007/s11587-021-00606-z.
27. Choi, S.U.S., 1995, *Enhancing thermal conductivity of fluids with nanoparticles*, Proc. of the ASME International Mechanical Engineering Congress and Exposition San Francisco, USA 1995, 66.
28. Abouelregal, A.E., Sedighi, H.M., Faghidian, S.A., Shirazi, A.H., 2021,*Temperature-dependent physical characteristic of the rotating nonlocal nanobeams subject to a varying heat source and a dynamic load*, FactaUniversitatis-Series Mechanical Engineering, 19(4), pp. 633-656.
29. Kameswaran, P.K., Narayana, M., Sibanda, P., Murthy, P.V.S.N., 2012, *Hydromagnetic nanofluid flow due to a stretching or shrinking sheet with viscous dissipation and chemical reaction effects*, *International Journal of Heat and Mass Transfer*, 55, pp. 7587-7595.
30. Xiong, Q., Altnji, S., Tayebi, T., Izadi, M., Hajjar, A., Sundén, B., Li, L.K., 2021, *A comprehensive review on the application of hybrid nanofluids in solar energy collectors*, Sustain. Energy Technol. Assess., 47, 101341.
31. Aneli, S., Gagliano, A., Tina, G.M., Hajji, B., 2020, *Analysis of the energy produced and energy quality of nanofluid impact on photovoltaic-thermal systems*. Proc. of the ICEERE 2nd International Conference on Electronic Engineering and Renewable Energy Systems, Saidia, Morocco 2020, pp. 739–745.
32. Abd Elazem, N.Y., Ebaid, A., 2017, *Effects of partial slip boundary condition and radiation on the heat and mass transfer of MHD-nanofluid flow*,Indian J. Phys., 91, pp. 1599–1608.
33. Abramowitz, M., Stegun, L.A., 1972, *Handbook of Mathematical Functions*, National Bureau of Standards, AMS 55.
34. Grubka, L.G., Bobba, K.M., 1985, *Heat transfer characteristics of a continuous stretching surface with variable temperature*, ASME J. Heat Transfer, 107, pp. 248–250.
35. Hamad, M.A.A., 2011, *Analytical solution of natural convection flow of a nanofluid over a linearly stretching sheet in the presence of magnetic field*, Int. Commun. Heat Mass Transfer, 38, pp. 487–492.
36. Noreen, S.A., Khan, Z.H., 2014, *Heat transfer study of an individual multiwalled carbon nanotube due to metachronal beating of cilia*, Int. Commun. Heat Mass Transfer, 59, pp. 114–119.
37. Abd Elazem, N.Y., 2016, *Numerical Solution for the Effect of Suction or Injection on Flow of Nanofluids Past a Stretching Sheet*, Z. Naturforsch. A, 71(6), pp. 511–515.
38. Elgazery, N.S., Abd Elazem, N.Y., 2011, *Effects of viscous dissipation and Joule heating for natural convection in a hydromagnetic fluid from heated vertical wavy surface*, Z. Naturforsch. A, 66(6-7), pp. 427 – 440.